Disruption of insulin receptor substrate-2 impairs growth but not insulin function in rats

Received for publication, February 19, 2020, and in revised form, July 1, 2020 Published, Papers in Press, July 6, 2020, DOI 10.1074/jbc.RA120.013095

Yuka Toyoshima[1,*], Katsuyuki Nakamura[2], Reiko Tokita[1], Naomi Teramoto[2], Hidetoshi Sugihara[2], Hisanori Kato[3], Keitaro Yamanouchi[2], and Shiro Minami[1]

From the [1]Department of Bioregulation, Institute for Advanced Medical Sciences, Nippon Medical School, Kosugi-machi, Nakahara-ku, Kawasaki, Japan, the [2]Department of Veterinary Physiology, Graduate School of Agricultural and Life Sciences, The University of Tokyo, Yayoi, Bunkyo-ku, Tokyo, Japan, and the [3]Department of Applied Biological Chemistry, Graduate School of Agricultural and Life Sciences, The University of Tokyo, Yayoi, Bunkyo-ku, Tokyo, Japan

Edited by Qi-Qun Tang

Insulin receptor substrate (IRS)-2, along with IRS-1, is a key signaling molecule that mediates the action of insulin and insulin-like growth factor (IGF)-I. The activated insulin and IGF-I receptors phosphorylate IRSs on tyrosine residues, leading to the activation of downstream signaling pathways and the induction of various physiological functions of insulin and IGF-I. Studies using IRS-2 knockout (KO) mice showed that the deletion of IRS-2 causes type 2 diabetes due to peripheral insulin resistance and impaired β-cell function. However, little is known about the roles of IRS-2 in other animal models. Here, we created IRS-2 KO rats to elucidate the physiological functions of IRS-2 in rats. The body weights of IRS-2 KO rats at birth were lower compared with those of their WT littermates. The postnatal growth of both male and female IRS-2 KO rats was also suppressed. Compared with male WT rats, the glucose and insulin tolerance of male IRS-2 KO rats were slightly enhanced, whereas a similar difference was not observed between female WT and IRS-2 KO rats. Besides the modestly increased insulin sensitivity, male IRS-2 KO rats displayed the enhanced insulin-induced activation of the mTOR complex 1 pathway in the liver compared with WT rats. Taken together, these results indicate that in rats, IRS-2 plays important roles in the regulation of growth but is not essential for the glucose-lowering effects of insulin.

The pleiotropic effects of insulin and insulin-like growth factor (IGF)-I on the regulation of somatic growth and a variety of metabolic functions are mediated by a complex network of intracellular signaling pathways (1). The insulin receptor substrate (IRS) proteins are intracellular adaptor proteins, and they are the main target proteins for the tyrosine kinase of insulin and IGF-I receptors (2, 3). After IRS proteins are tyrosine-phosphorylated by the activated insulin and IGF-I receptors, they interact with the signaling molecules and transmit the signals to downstream machinery, including the phosphatidylinositol 3-kinase (PI3K) pathway and the mTOR complex 1 (mTORC1) pathway.

In mammals, IRS-1 and IRS-2 are major substrates for insulin and IGF-I receptors and are widely expressed (2, 3). They both contain a pleckstrin homology (PH) domain, a phosphotyrosine-binding (PTB) domain, and a C-terminal region, including the potential residues of tyrosine for phosphorylation by the activated insulin/IGF-I receptor. The PH and PTB domains mediate the associations with the activated insulin/IGF-I receptor (4, 5). Despite these substrates' similar structures, the physiological functions of IRS-2 differ from those of IRS-1, as has been demonstrated using knockout (KO) mouse models.

In mice, IRS-2 deficiency does not affect growth, but it causes type 2 diabetes as a result of hepatic insulin resistance and the loss of β-cell function by 10 weeks of age (6–8). In contrast, mice lacking IRS-1 are growth-retarded at the embryonic and postnatal periods and display insulin resistance (especially in skeletal muscle and adipose tissue), but they do not develop type 2 diabetes because of the adequate insulin secretion from β-cells (9–11). These findings indicate that IRS-2 and IRS-1 play distinct roles in the regulation of glucose homeostasis; however, the available data are limited to mice due to the difficulties of gene targeting in other animals.

The discovery of the clustered regulatory interspaced short palindromic repeats (CRISPR)/CRISPR-associated nuclease (Cas)9 system made it possible to produce gene knockout models of many species, including rats (12–15). In the present study, we generated IRS-2 KO rats by using the CRISPR/Cas9 system to determine the physiological functions of IRS-2 in rats.

Results

The generation of IRS-2 knockout rats using the CRISPR/Cas9 system

The PCR amplification of targeting loci and the subsequent sequencing analysis confirmed the mutations of the F0 rats, but IRS-2 protein was expressed in all F0 rats because they had an allele of WT, 1-base pair (bp) insertion, or a 3-bp deletion upstream of the start codon of *Irs-2* gene. We then chose two male F0 rats that had either a 4,099-bp deletion (mutation 1) or a 363-bp deletion (mutation 2) to establish the colonies (Fig. 1, *A* and *B*). Because these deletions include the start codon, the translation of short-length IRS-2–like protein could occur by using an alternative ATG located downstream of the annotated start codon.

However, the RT-PCR analysis did not detect either fragment 1 (*Irs-2*_1) or fragment 2 (*Irs-2*_2) of IRS-2 mRNA in the

This article contains supporting information.

* For correspondence: Yuka Toyoshima, toyoshima.yuka@ocha.ac.jp.
Present address for Yuka Toyoshima: Institute for Human Life Innovation, Ochanomizu University, Otuska, Bunkyo-ku, Tokyo, Japan.

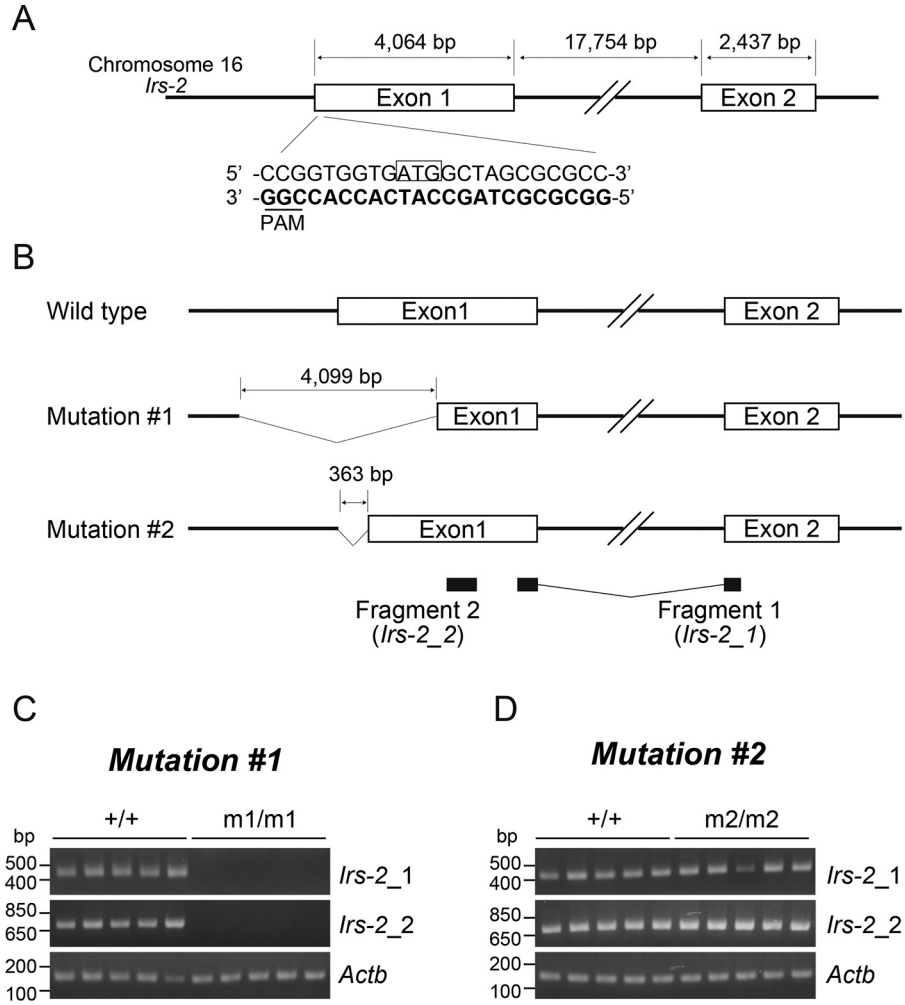

Figure 1. Generation of *Irs-2*–mutated rats with CRISPR/Cas9. *A,* the structure of rat *Irs-2* gene and the target loci of *Irs-2*. The sgRNA sequence is shown in *bold*, and the protospacer adjacent motif (*PAM*) is *underlined*. The annotated start codon of *Irs-2* is *boxed*. *B,* the structure of mutations 1 and 2. The *black bars* represent the locations of the fragments 1 and 2 of *Irs-2* (*Irs-2*_1 and *Irs-2*_2), which was detected by the RT-PCR analysis. *C* and *D,* the RT-PCR analysis for *Irs-2*_1, *Irs-2*_2, and *Actb* expression in the brain of 15-week–old WT (+/+) rats and homozygous rats with mutation 1 (m1/m1) (*C*) or mutation 2 (m2/m2) (*D*).

brains of the homozygous rats with mutation 1 (Fig. 1*C*), indicating that IRS-2-like mRNA was not expressed in these rats. In addition, the immunoblot analysis of the total protein and that of the immunoprecipitated IRS-2 protein from the brains and epididymal white adipose tissues (epiWAT) of the homozygous rats with mutation 1 confirmed the absence of IRS-2 protein (Fig. 2, *A* and *B*). In the brains of the homozygous rats with mutation 2, both fragment 1 (*Irs-2*_1) and fragment 2 (*Irs-2*_2) of IRS-2 mRNA expression were apparent (Fig. 1*D*), and a low level of short-length IRS-2–like protein (approximately 122 kDa) was expressed; this protein could be the product with a deletion of the PH domain and one-half of a PTB domain predicted from the sequence (Fig. 2, *C* and *D*). In the epiWAT of the homozygous rats with mutation 2, the truncated IRS-2 protein was also expressed (Fig. 2*C*), but it was not clearly detected in the immunoprecipitated IRS-2 protein samples (Fig. 2*D*). The levels of IRS-1 protein in the brain and epiWAT were comparable between the WT and mutant rats of both lines (Fig. 2, *A* and *C*). In light of these results, we decided to use the mutation 1 line as KO rats for further experiments.

The disruption of IRS-2 impaired growth

At 1–2 days after birth, the neonate KO rats had 25–30% lower body weights (BWs) compared with the WT (WT) and heterozygous (hetero) rats (WT: 7.1 ± 1.0 g; hetero: 6.5 ± 0.8 g; KO: 5.0 ± 0.5 g). Among the males, the lower BWs of the KO rats persisted until after weaning (Fig. 3*A*), and at 15 weeks of age the BWs of the KO rats were approximately 65% of those of the WT rats (Table S1). During the experimental period, there was no difference in BW between the WT and heterorats.

At 15 weeks of age, the body length was significantly shorter in the male KO rats compared with the male WT rats (Fig. 3, *B* and *C*). The weights of the liver, gastrocnemius muscle, kidney, brain, and epidydimal fat pad were significantly lower in the male KO rats compared with the male WT rats (Table S1), and the ratio of these tissues' weights to the BW (%), except for gastrocnemius muscle, were also significantly lower in the male KO rats than in the male WT rats (Fig. 3*D*). The serum growth hormone (GH) and IGF-I levels were significantly lower in the male KO rats *versus* the male WT rats (Fig. 4, *A* and *B*).

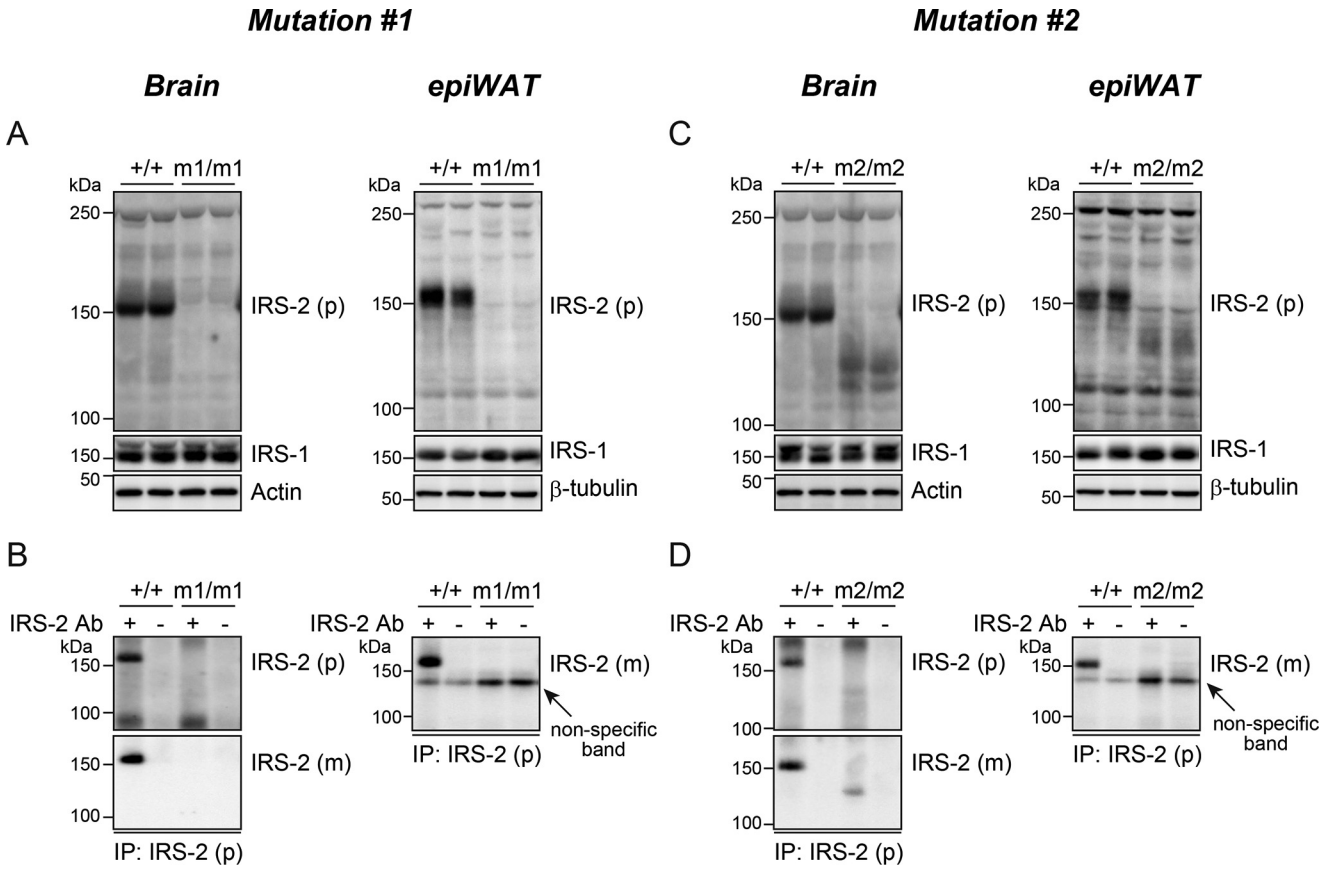

Figure 2. The IRS-2 protein expression in the 15-week–old *Irs-2*–mutated rats. *A–D*, the IRS-2 protein level in the brain and epiWAT of WT (+/+) rats and homozygous rats with mutation 1 (m1/m1) (*A* and *B*) or mutation 2 (m2/m2) (*C* and *D*). *A* and *C*, total brain and epiWAT homogenates were analyzed by immunoblotting with antibodies against IRS-1, IRS-2, actin, and β-tubulin. Actin and β-tubulin were used as an internal control. A representative immunoblot of IRS-2 was detected using polyclonal anti-IRS-2 antibody (*IRS-2 (p)*). *B* and *D*, the immunoprecipitated IRS-2 from the brain homogenates was analyzed by immunoblotting with polyclonal (*IRS-2 (p)*) and monoclonal (*IRS-2 (m)*) anti-IRS-2 antibodies. The immunoprecipitated IRS-2 from the epiWAT homogenates was analyzed by immunoblotting with anti-IRS-2 (*IRS-2 (m)*) antibody.

Among the females, the KO rats also showed attenuated BW gain (Fig. 3*E*) and shorter body lengths compared with the WT rats, as in the males (Fig. 3, *F* and *G*). The weights of the liver, gastrocnemius muscle, kidney, and brain were significantly lower in the female KO rats compared with the female WT rats (Table S1), and the ratio of these tissues' weights to BW (%), except for gastrocnemius muscle, were significantly lower in the female KO rats than in the female WT rats (Fig. 3*H*). In contrast to the reduced levels of GH and IGF-I in the KO males, the serum GH level was comparable between the female WT and KO rats (Fig. 4*C*), and the serum IGF-I level was significantly higher in the female KO rats than in the female WT rats (Fig. 4*D*). A similar reduction of BW was observed in male and female rats carrying mutation 2 despite the incomplete deletion of IRS-2 in that line (Fig. S1).

The disruption of IRS-2 did not impair glucose tolerance or insulin sensitivity

IRS-2–deficient mice have exhibited glucose intolerance and insulin resistance by 10 weeks of age (6, 7). We therefore performed a glucose tolerance test (GTT) and a insulin tolerance test (ITT) to evaluate the glucose metabolism and insulin sensitivity in 11- to 13-week–old male and female KO rats. During the GTT, the male WT and KO rats showed peak blood glucose levels at 15 min after the glucose administration, and this level was significantly lower in the male KO rats compared with the male WT rats (Fig. 5*A*). The incremental area under the glucose curve (AUC) during the GTT was slightly but significantly lower in the male KO rats *versus* the male WT rats (Fig. 5*B*), indicating that glucose tolerance was slightly enhanced in the male KO rats compared with the male WT rats. The plasma insulin levels before and after the glucose injection tended to be lower in the male KO rats than in the male WT rats, but these differences did not reach significance (Fig. 5, *C* and *D*).

During the ITT, the male KO rats had slightly but significantly higher fasting blood glucose levels; however, their blood glucose levels at 120 min after the insulin injection tented to be lower than that observed in the male WT rats ($p = 0.07$, Fig. 5*E*). The area above the curve (AAC) for the changes of blood glucose levels during the ITT was significantly higher in the male KO rats than in the male WT rats (Fig. 5*F*), indicating that insulin sensitivity was enhanced in the male KO rats. Similar GTT and ITT results were observed in the male WT and KO rats at 27–28 weeks of age (Fig. S2).

Unlike the male KO rats, the female KO rats exhibited glucose and insulin tolerance that was similar to that of the female WT rats at 11–13 weeks of age (Fig. 6, *A–F*), although there

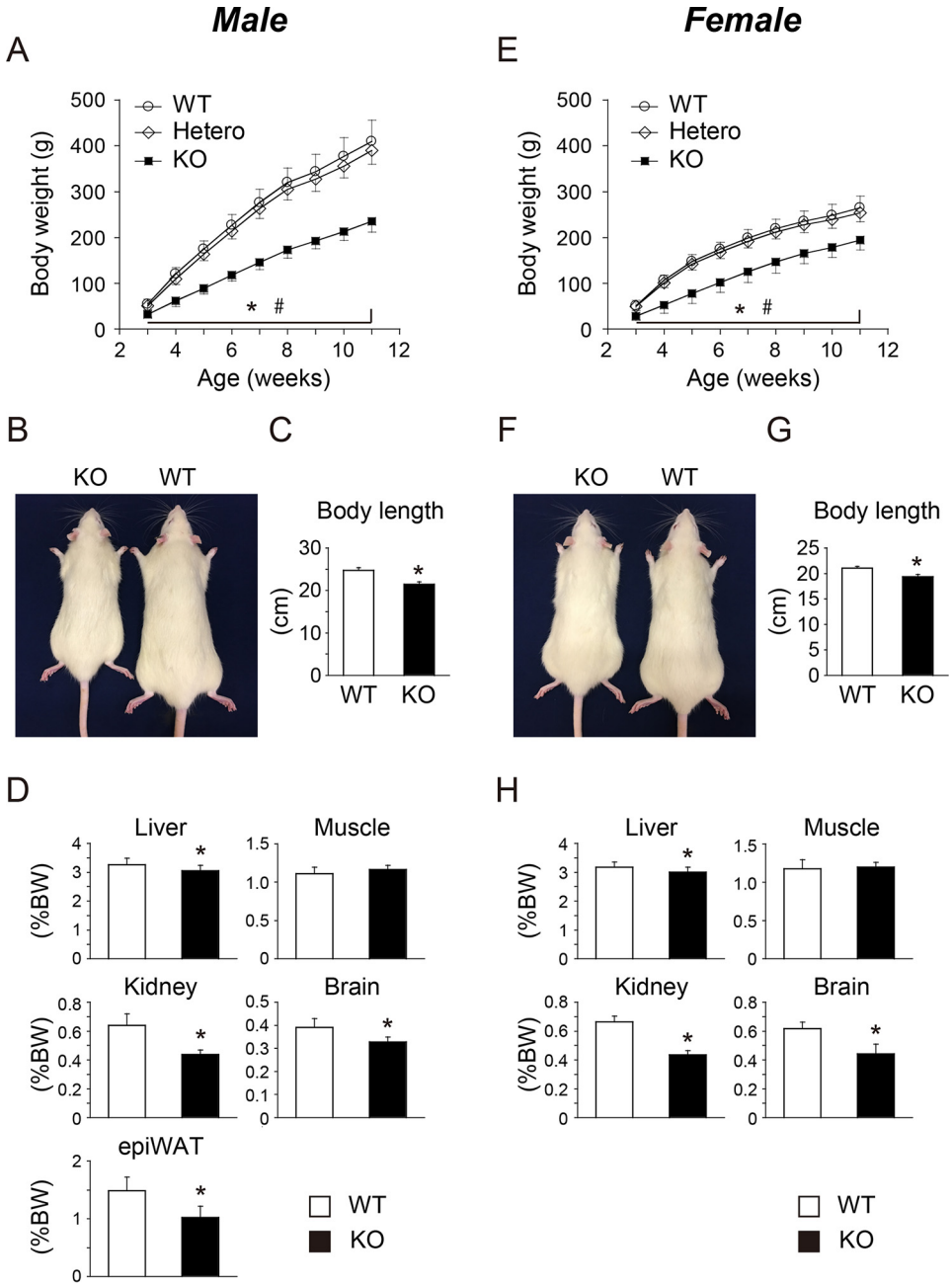

Figure 3. BW, body length, and organ weights in IRS-2 KO rats. *A,* the changes of BW in male WT ($n = 12$), heterozygous (*hetero*; $n = 13$), and IRS-2 knockout (KO; $n = 11$) rats from 3 to 11 weeks of age. *B,* a male KO rat and a male WT littermate at 15 weeks of age. *C,* the body length in 15-week–old male WT ($n = 13$) and KO ($n = 12$) rats. The body length was measured as the distance from nose tip to anus. *D,* the weights of the liver, gastrocnemius muscle, kidney, brain, and epiWAT per BW in 15-week–old male WT ($n = 13$) and KO ($n = 12$) rats. *E,* the changes of BW in 3- to 11-week–old female WT ($n = 13$), hetero ($n = 13$), and KO ($n = 12$) rats. *F,* a female KO rat and a female WT littermate at 15 weeks of age. *G,* the body length in 15-week–old female WT ($n = 13$) and KO ($n = 12$) rats. *H,* the weights of the liver, gastrocnemius muscle, kidney, and brain per BW in female WT ($n = 13$) and KO ($n = 12$) rats. Values are mean ± S.D. *, $p < 0.05$ *versus* WT rats; #, $p < 0.05$ *versus* Heterorats.

was a small difference in the changes in the blood glucose level at 15 min during the GTT (Fig. 6*A*). The 27- to 28-week–old female KO rats had significantly higher plasma insulin levels at 15 min after the glucose injection compared with the female WT rats, and they maintained normal blood glucose levels during the GTT (Fig. S3, *A–D*). In the ITT, the changes in the blood glucose level were similar in the WT and KO females, although the calculated AAC was slightly increased in the female KO rats (Fig. S3, *E* and *F*).

The disruption of IRS-2 did not change the insulin-induced tyrosine phosphorylation of insulin receptor (IR) and IRS-1 in the liver and skeletal muscle

Because the male KO rats showed a small enhancement of insulin sensitivity, we next investigated the early steps of insulin signaling in the liver and skeletal muscle of both WT and KO males. Our results first showed that there was no increase in the tyrosine phosphorylation of IRS-2 or in the activation of IRS-2–associated PI3K in the liver and skeletal muscle of KO males (Fig. 7).

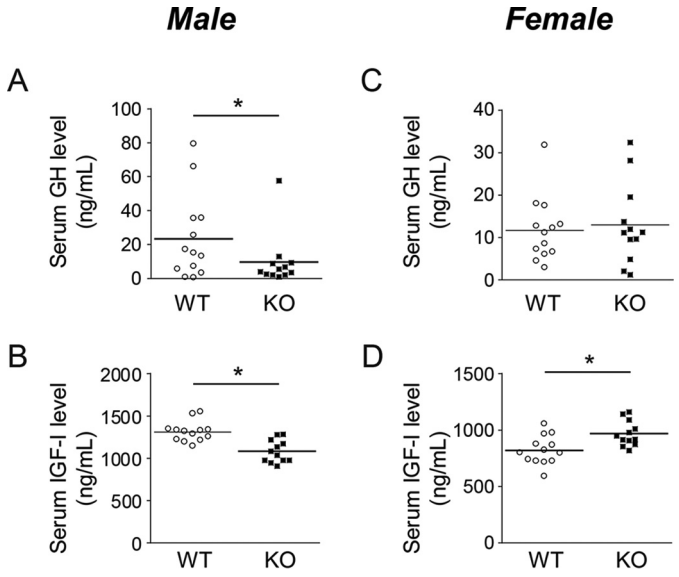

Figure 4. Serum GH and IGF-I in IRS-2 KO rats. *A* and *B*, serum GH (*A*) and IGF-I (*B*) levels in 15-week–old male WT ($n = 13$) and KO ($n = 12$) rats. *C* and *D*, serum GH (*C*) and IGF-I (*D*) levels in 15-week–old female WT ($n = 13$) and KO ($n = 12$) rats. Values are mean ± S.D. *, $p < 0.05$ *versus* WT rats.

In the liver, insulin significantly increased the tyrosine phosphorylation of insulin receptor β-subunit (IRβ) and IRS-1 in both WT and KO rats, but the absence of IRS-2 did not affect the levels of this insulin-induced phosphorylation (Fig. 8, *A* and *B*). Similarly, insulin caused comparable activations of IRS-1–associated PI3K in the livers of male WT and KO rats (Fig. 8, *C* and *D*).

Similar to the liver, in skeletal muscle, insulin significantly increased the tyrosine phosphorylation of IRβ and IRS-1, and there was no effect of the deletion of *Irs-2* gene on the levels of this insulin-induced phosphorylation observed in the male WT and KO rats (Fig. 8, *E* and *F*). In contrast, a marginally significant reduction of the insulin-stimulated activity of PI3K associated with IRS-1 was seen in the skeletal muscle of the male KO rats compared with the male WT rats (Fig. 8, *G* and *H*).

The disruption of IRS-2 enhanced the insulin-induced activation of the mTORC1 pathway in the liver of KO rats

We then examined insulin signaling downstream of PI3K in the liver and skeletal muscle of male WT and KO rats. In the liver, insulin significantly increased phosphorylation of Akt, GSK3β, and S6K (Fig. 9, *A–D*). The absence of IRS-2 did not affect the insulin-stimulated phosphorylation levels of Akt and GSK3β (Fig. 9, *A–C*), whereas the insulin-stimulated phosphorylation level of S6K, a substrate of mTORC1, was significantly higher in the KO rats than in the WT rats (Fig. 9, *A* and *D*). Because the mTORC1/S6K pathway is shown to be involved in the feedback regulation by insulin through serine (Ser)/threonine (Thr) phosphorylation of IRS-1 (16), phosphorylation of IRS-1 at Ser-307, a site phosphorylated by mTORC1/S6K pathway in response to insulin (17–20), was examined as well as its tyrosine phosphorylation. Insulin significantly increased the Ser-307 and tyrosine phosphorylation of IRS-1 in both WT and KO rats (Fig. 9, *E–G*). Despite the higher phosphorylation level of S6K in the liver of KO rats (Fig. 9, *A* and *D*), insulin-stimulated Ser-307 and tyrosine phosphorylation levels of IRS-1 in the liver were comparable with WT rats (Fig. 9, *E–G*).

In the skeletal muscle, insulin significantly increased the phosphorylation of Akt, G3K3β, and S6K in the male WT and KO rats (Fig. 10, *A–D*). Despite the reduced insulin-induced IRS-1–associated PI3K activity, no effect of the deletion of IRS-2 was observed in the levels of these insulin-stimulated phosphorylation (Fig. 10, *B–D*).

Discussion

In the present study, we created IRS-2 KO rats by using the CRISPR/Cas9 system, and we analyzed the rats phenotypes'. The genetic disruption of IRS-2 resulted in the inhibition of growth in rats, but it did not impair glucose tolerance or insulin sensitivity until 28 weeks of age. Moreover, the male IRS-2 KO rats showed slightly increased insulin sensitivity along with an up-regulation of insulin signaling through the mTORC1 pathway in the liver. These results indicate that in rats, IRS-2 plays critical roles in the regulation of growth but not in the glucose-lowering effect of insulin. Similar results were obtained using two independent lines of IRS-2 KO rats (carrying mutation 1 and mutation 2), supporting the concept that these phenotypes were specific for the deficiency of full-length IRS-2 protein.

Both male and female IRS-2 KO rats had lower BWs and shorter body lengths compared with the WT rats during the postnatal period up to 15 weeks of age. Compared with the male WT rats, the male IRS-2 KO rats had lower levels of serum GH and IGF-I, two major hormones regulating growth (21), whereas the female IRS-2 KO rats had similar serum GH levels and rather higher IGF-I levels compared with the female WT rats. These results suggest that the changes in the levels of these hormones were not primary causes of the growth inhibition induced by deletion of the *Irs-2* gene in rats. The IGF-I signaling and its actions could be attenuated in IRS-2 KO males and females. In addition, the reduction of the serum levels of GH and IGF-I could have contributed to the more severe growth inhibition phenotype in the males compared with the females.

In addition to the BWs, the weights of the liver, gastrocnemius muscle, kidney, and brain were also lower in both the male and female IRS-2 KO rats compared with the corresponding WT rats. Of these tissues, the weights of the kidney and brain normalized to the BW were much lower in the IRS-2 KO rats than in the WT rats. In contrast, the deletion of IRS-2 had a smaller effect on the normalized liver weights and no effect on the gastrocnemius muscle weights normalized to BW. These findings imply that IRS-2 is important for the control of kidney and brain growth but not for skeletal muscle growth.

Previous studies have shown that IRS-2 KO mice develop type 2 diabetes by 10 weeks of age as a result of hepatic insulin resistance and inadequate compensatory insulin secretion due to impaired β-cell hyperplasia (6, 7, 22–24). From these data, we speculated that the IRS-2 KO rats would also develop type 2 diabetes; however, they did not show glucose intolerance or insulin resistance up to 28 weeks of age. The data showing the changes in the plasma insulin levels during the GTT imply that the insulin secretion in IRS-2 KO rats was nearly normal. These results indicate that the deletion of IRS-2 did not impair

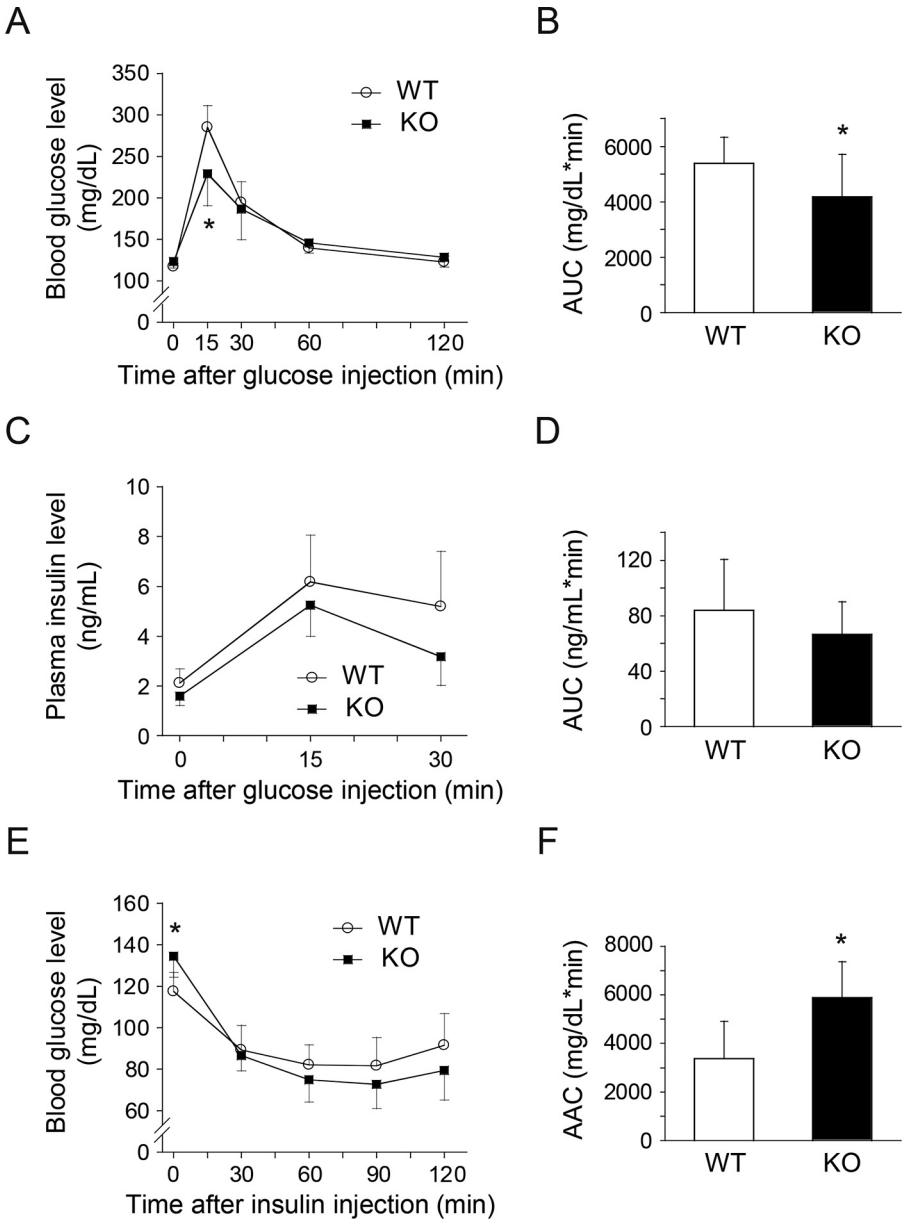

Figure 5. GTT and ITT in 11- to 13-week–old male WT and IRS-2 KO rats. *A–D*, the GTT results for the 11- to 12-week–old WT ($n = 11$) and KO ($n = 11$) rats. *A*, the changes in blood glucose levels during the GTT. *B*, the incremental AUC for the blood glucose level during the GTT. *C*, the changes in plasma insulin levels during the GTT. *D*, the incremental AUC for the plasma insulin level during the GTT. *E* and *F*, the ITT results of the 12- to 13-week–old WT ($n = 10$) and KO ($n = 12$) rats. *E*, the changes in the blood glucose levels during the ITT. *F*, the AAC for the blood glucose level during the ITT. Values are mean ± S.D. *, $p < 0.05$ *versus* WT rats.

glucose tolerance or insulin sensitivity in rats. The islet morphology was also examined, and the results showed that despite the small impacts on the islet size, the total number of islets observed in all sections was fewer in IRS-2 KO rats than in WT rats at 15 weeks of age (Fig. S4) (supporting Materials and Methods). Collectively, these results suggest that IRS-2 KO could maintain normal insulin secretion with fewer pancreatic islets compared with the WT rats.

In addition, in the male rats, deletion of the *Irs-2* gene yielded a subtle but significant enhancement of insulin sensitivity together with increased activation of the hepatic mTORC1 pathway in response to insulin. We also examined whether the enhancement of insulin-induced activation of the mTORC1 pathway could increase Ser/Thr phosphorylation of IRS-1 as the feedback regulation of insulin in the liver of IRS-2 KO rats. Because Ser/Thr phosphorylation of IRS-1 is shown to inhibit its tyrosine phosphorylation and mediate insulin resistance (16, 25), it is possible that the enhanced mTORC1 pathway attenuates insulin signaling via IRS-1 in the liver of IRS-2 KO rats. Thus far, many Ser/Thr phosphorylation sites of the IRS-1 protein have been reported (16, 25). Of these sites, we analyzed phosphorylation of IRS-1 at Ser-307 that is known to be regulated by the mTORC1 pathway in response to insulin (17–20). The data showed that the absence of IRS-2 did not affect insulin-induced Ser-307 phosphorylation of IRS-1 in the liver as well as its tyrosine phosphorylation, suggesting that enhancement of insulin-induced activation of the mTORC1 pathway is not involved in the negative-feedback regulation of insulin

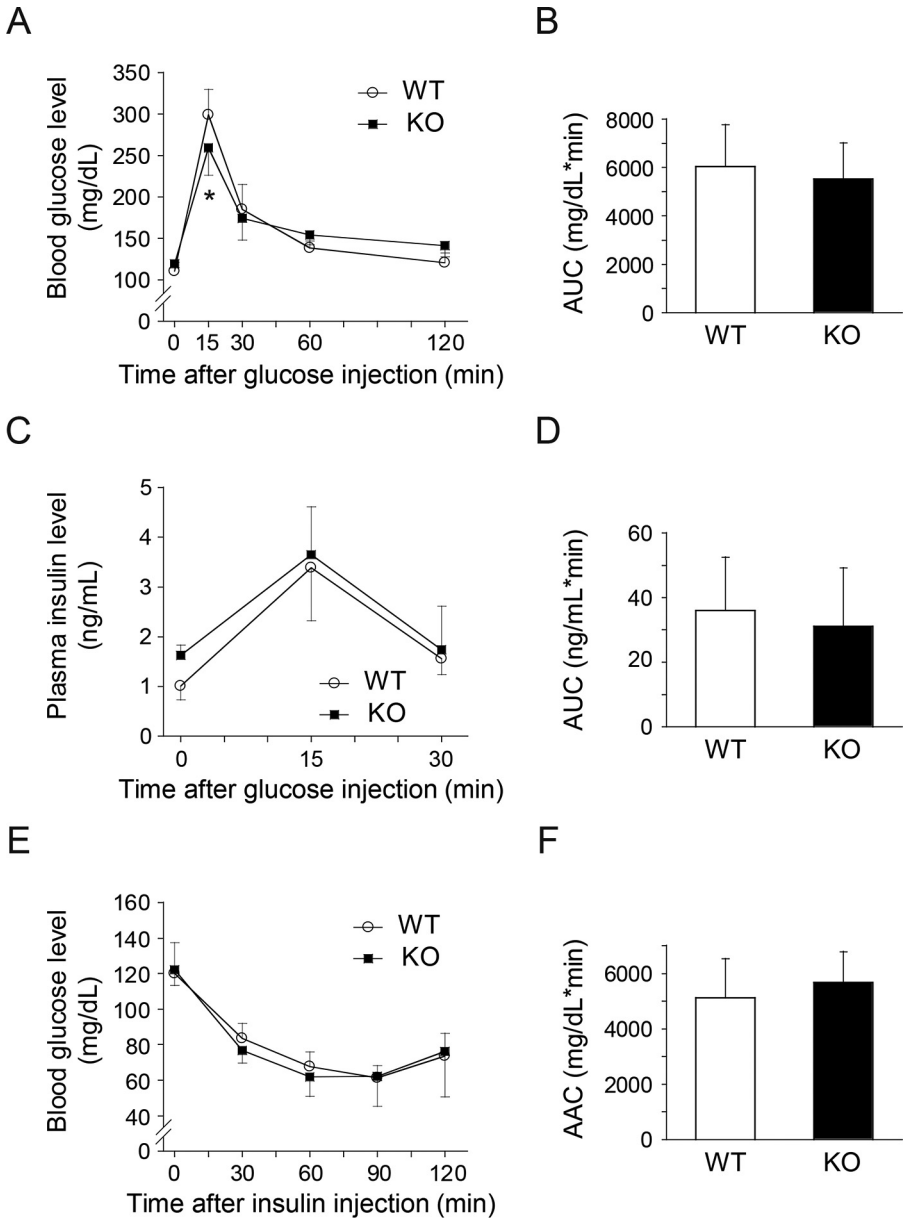

Figure 6. The GTT and ITT results of the 11- to 13-week–old female WT and IRS-2 KO rats. *A–D*, the GTT results for the 11- to 12-week–old WT ($n = 9$) and KO ($n = 12$) rats. *A*, the changes in blood glucose levels during the GTT. *B*, the incremental AUC for the blood glucose level during the GTT. *C*, the changes in plasma insulin levels during the GTT. *D*, the incremental AUC for the plasma insulin level during the GTT. *E* and *F*, the ITT results for the 12- to 13-week–old WT ($n = 11$) and KO ($n = 12$) rats. *E*, the changes in blood glucose levels during the ITT. *F*, the AAC for the blood glucose level during the ITT. Values are mean ± S. D. *, $p < 0.05$ *versus* WT rats.

signaling via IRS-1. Taken together, the enhanced hepatic mTORC1 pathway in response to insulin could contribute to the increase in insulin sensitivity in IRS-2 KO rats.

The overall phenotypes of the IRS-2 KO rats showed the difference between the sexes. The growth defect induced by the lack of IRS-2 was more severe in males than in the females. The modifications of glucose tolerance between the sexes were also distinct. Despite the normal glucose tolerance in the male and female IRS-2 KO rats, the plasma insulin level during the GTT was lower in the male IRS-2 KO rats than in the male WT rats, but it was higher in the female IRS-2 KO rats than in the female WT rats, especially at older ages. The male IRS-2 KO rats exhibited small but significant enhancement of insulin sensitivity and a higher level of insulin-induced S6K phosphorylation in the liver compared with the male WT rats, whereas the female IRS-2 KO rats did not exhibit these alterations (Fig. 6 and Fig. S5). Sexual dimorphism has also been observed in IRS-2 KO mice; male IRS-2 KO mice developed type 2 diabetes, whereas female IRS-2 KO mice did not (7). In addition, female IRS-2 KO mice are infertile because of the defects in the hypothalamic reproductive endocrine system, but this phenotype has not been observed in males (26). Further studies are necessary to identify the reasons for the sex differences induced by deletion of the *Irs-2* gene in these animal models.

Although the effects of *Irs-2* gene deletion on body growth and glucose metabolism differ between rats and mice, smaller than normal brain sizes were commonly observed in both rats and mice lacking IRS-2. In IRS-2 KO mice, all brain regions

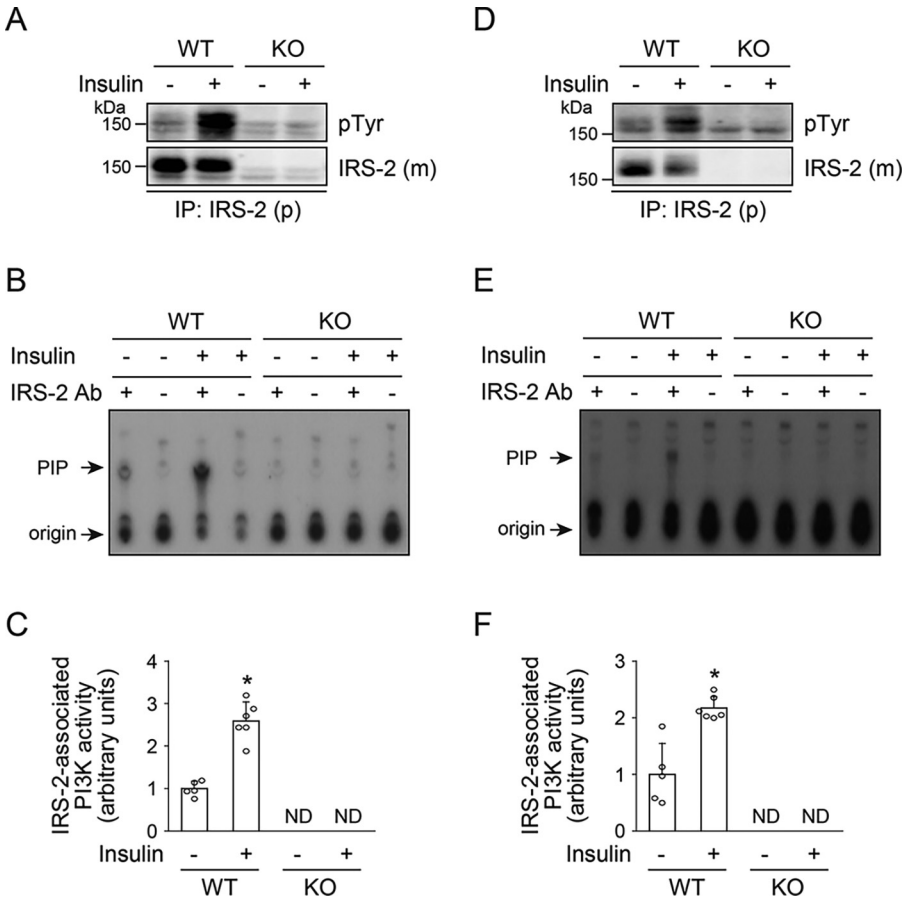

Figure 7. The insulin-simulated tyrosine phosphorylation of IRS-2 and activation of PI3K associated with IRS-2 in the liver and skeletal muscle of male WT and IRS-2 KO rats. The 8-week–old male WT and KO rats were fasted overnight, and insulin or vehicle was subsequently injected into the inferior vena cava. The liver was dissected at 1 min and skeletal muscle was dissected at 2 min after the insulin injection. *A,* representative immunoblots of the insulin-stimulated tyrosine phosphorylation of IRS-2 in the liver. The immunoprecipitated IRS-2 from the liver homogenates was analyzed by immunoblotting with anti-phosphotyrosine (*pTyr*) and monoclonal anti-IRS-2 (*IRS-2(m)*) antibodies. *B* and *C,* the IRS-2-associated PI3K activity in the liver. *B,* a representative autoradiograph. *C,* the quantification of radioactivity incorporated into phosphatidylinositol (PIP). *D,* representative immunoblots of the insulin-stimulated tyrosine phosphorylation of IRS-2 in the skeletal muscle. The immunoprecipitated IRS-2 from the skeletal muscle homogenates was analyzed by immunoblotting with anti-pTyr and anti-IRS-2 (*IRS-2(m)*) antibodies. *E* and *F,* the IRS-2-associated PI3K activity in the skeletal muscle. *E,* a representative autoradiograph. *F,* the quantification of radioactivity incorporated into PIP. Values are mean ± S.D. WT and KO with −insulin groups, $n = 5$. WT and KO with +insulin groups, $n = 6$. *, $p < 0.05$ *versus* WT rats with −insulin.

were smaller than those of WT mice, but the brain structure was normal (27). The functions of brain IRS-2 have been elucidated by using tissue-specific IRS-2 KO mice (28). However, the roles of IRS-2 in neurodegeneration and cognition are a matter of controversy. Some studies showed that the lack of brain IRS-2 delayed the progression of neurodegeneration and increased hippocampal memory formation (29, 30), whereas other studies indicated that it caused an impairment of *N*-methyl-D-aspartate receptor-dependent synaptic plasticity and long-term potentiation in hippocampal neurons (31, 32). The IRS-2 KO rats and the future generation of brain-specific IRS-2 KO rats are likely to be useful in studies designed to clarify these contradictions.

In conclusion, our present data demonstrate that in rats, the genetic deletion of IRS-2 reduced body growth and did not impair glucose tolerance or insulin sensitivity. These data indicate that IRS-2 is important in rats for the regulation of growth but is not essential for the glucose-lowering effects of insulin. Further studies using a variety of animal models targeting the IRS proteins are necessary to determine the proteins' physiological functions and their roles in insulin/IGF-I signaling.

Experimental procedures

Animals

For all of the animal experiments, the rats were kept in a room maintained at 22 ± 2 °C with relative humidity at 40–60% and a 12-h light (8:00–20:00) and 12-h darkness (20:00–8:00) cycle. They were allowed free access to water and a standard chow (MF; Oriental Yeast, Tokyo). All experimental procedures were in accord with the guidelines of the Animal Usage Committee of Nippon Medical School and were verified by the Committee.

The generation of IRS-2 mutant rats with the CRISPR/Cas9 system

IRS-2 mutant rats were generated with the CRISPR/Cas9 system. The design of single guide (sg) RNA for targeting the rat *Irs-2* gene and the preparation of sgRNA and Cas9 mRNA were conducted as described (33). The sequence of sgRNA is shown in Fig. 1*A*. The injection of Cas9 mRNA and sgRNA was performed as described with some modification (34). Briefly, 25 IU of equine chorionic gonadotropin was intraperitoneally injected into 4- to 5-week–old sexually immature female Wistar-Imamichi rats

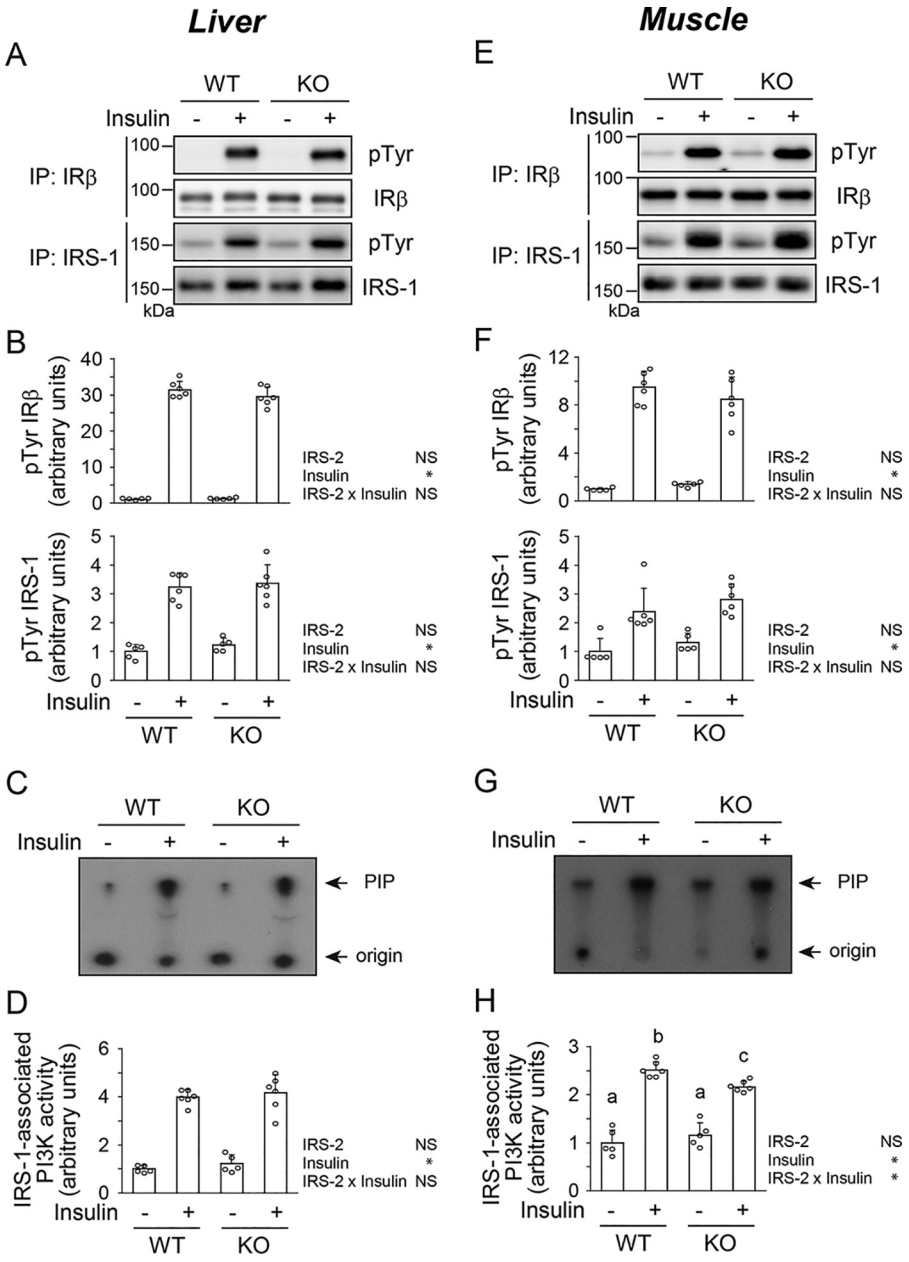

Figure 8. The insulin-simulated tyrosine phosphorylation of IRβ and IRS-1 and the activation of PI3K associated with IRS-1 in the liver and skeletal muscle of male WT and IRS-2 KO rats. The 8-week–old male rats were treated as described in the legend to Fig. 7. *A* and *B,* insulin-stimulated tyrosine phosphorylation of IR*β* and IRS-1 in the liver. The immunoprecipitated IR*β* or IRS-1 from the liver homogenates was analyzed by immunoblotting with anti-phosphotyrosine (*pTyr*), anti-IR*β*, and anti-IRS-1 antibodies. *A,* representative immunoblots. *B,* the ratio of pTyr to the amount of immunoprecipitated IR*β* (*upper graph*) or IRS-1 (*lower graph*). The immunoreactivity of pTyr was quantified and divided by the immunoreactivity of IR*β* or IRS-1. *C* and *D,* insulin-stimulated PI3K activity in the liver. *C,* a representative autoradiograph. *D,* the quantification of radioactivity incorporated into PIP. *E* and *F,* insulin-stimulated tyrosine phosphorylation of IR*β* and IRS-1 in skeletal muscle. *E,* representative immunoblots. *F,* the ratio of pTyr to the amount of immunoprecipitated IR*β* (*upper graph*) or IRS-1 (*lower graph*). *G* and *H,* insulin-stimulated PI3K activity in skeletal muscle. *G,* a representative autoradiograph. *H,* the quantification of radioactivity incorporated into PIP. Values are mean ± S.D. WT and KO with −insulin groups, $n = 5$. WT and KO with +insulin groups, $n = 6$. The two-way ANOVA results are next to the graph (*, $p < 0.05$, *NS,* not significant). Significant differences ($p < 0.05$) between values are indicated with different letters (*a*, *b*, etc.) when there was a significant interaction of genotype and insulin.

(The Institute for Animal Production, Ibaraki, Japan) to promote follicle maturation. At 48 h after the equine chorionic gonadotropin injection, these rats were intraperitoneally injected with 25 IU of human chorionic gonadotropin to induce ovulation and mated with male Wistar rats (Charles River Japan, Kanagawa, Japan) overnight. The pseudopregnant Wistar-Imamichi rats were prepared by manual vaginocervical stimulation with a glass rod at the proestrous stage. The next day, superovulated zygotes were collected from the female rats' oviducts, treated with hyaluronidase (Sigma-Aldrich), washed, and cultured in M2 medium (Sigma-Aldrich) until the microinjection: approximately 4 pl of a mixture of 50 mg/ml of sgRNA and 50 mg/ml of Cas9 mRNA were injected into the zygotic cytosol with a microinjector (Narishige, Tokyo). After injection, the zygotes were recovered in M16 medium (Sigma-Aldrich) for 1 h and transferred to the oviductal ampullas of the pseudopregnant Wistar-Imamichi rats.

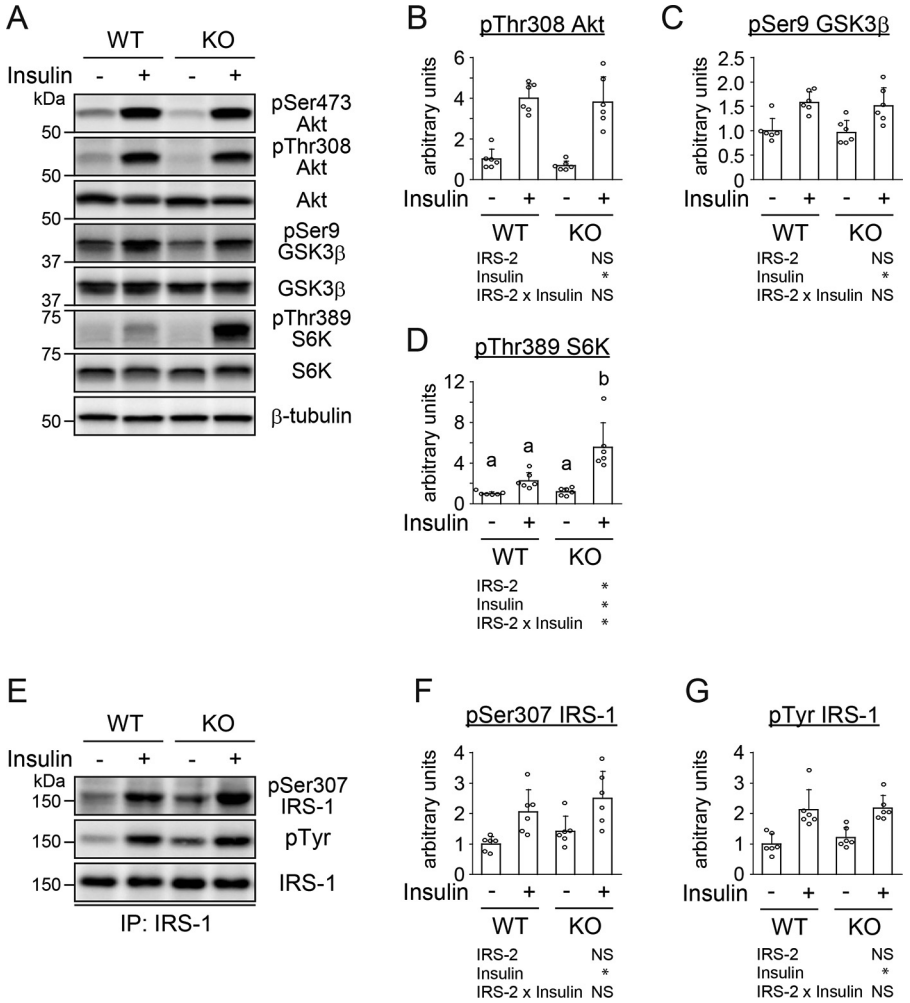

Figure 9. The insulin-simulated phosphorylation of Akt, GSK3β, S6K, and IRS-1 on Ser-307 in the liver of male WT and IRS-2 KO rats. The 8-week–old male rats were treated as described in the legend to Fig. 7, and the liver was dissected at 15 min after the insulin injection. *A–D*, insulin-stimulated phosphorylation of Akt, GSK3*β*, and S6K in the liver. *A,* representative immunoblots. *B–D*, the immunoreactivity of Thr-308 phosphorylation of Akt (*B*), Ser-9 phosphorylation of GSK3*β* (*C*), and Thr-389 phosphorylation of S6K (*D*) was quantified and divided by the immunoreactivity of *β*-tubulin. *E–G*, insulin-stimulated Ser-307 and tyrosine phosphorylation of IRS-1 in the liver. The immunoprecipitated IRS-1 from the liver homogenates was analyzed by immunoblotting with anti-phospho–Ser-307 IRS-1 (*pSer307 IRS-1*), and anti-phosphotyrosine (pTyr) antibodies. *E,* representative immunoblots. *F,* the ratio of pSer-307 IRS-1 to the amount of immunoprecipitated IRS-1. *G,* the ratio of pTyr to the amount of immunoprecipitated IRS-1. Values are mean ± S.D. ($n = 6$). The two-way ANOVA results are below the graph (*, $p < 0.05$, *NS,* not significant). Significant differences ($p < 0.05$) between values are indicated with different letters (*a*, *b*, etc.) when there was a significant interaction of genotype and insulin.

After F0 rats were born, PCR was performed with the genomic DNA extracted from the rats' tail tips. The purified PCR products were directly sequenced or sequenced after TA cloning to determine the mutations in *Irs-2* gene. We checked the off-target effects in F0 rats by PCR and sequencing analyses and confirmed that the rats did not have any mutations in the potential off-target sites. We selected two male F0 rats that had either mutation 1 or 2 (Fig. 1*B*) for the expansion of colonies.

Genotyping and breeding

Rats were genotyped by PCR. The primer sequences used were as follows: 5′-AGCGGCCACAAGACAGTGTG-3′ and 5′-TGTGGCAGCTGTTGCTGGAG-3′ for the line of mutation 1; 5′-CTCGGTGCGCGATGTGTTAC-3′ and 5′-GACGGCTGTTCGCAATTGAG-3′ for the line of mutations 1 and 2. All rats used in this study were maintained on a Wistar × Wistar Imamichi hybrid background. Male and female heterozygous rats having either mutation 1 or 2 were intercrossed to obtain homozygous littermates. To perform each experiment using enough numbers of each genotype of rats, approximately 20 mating pairs were set up simultaneously, and several littermates were pooled.

At 15 weeks of age, after having fasted for 4–5 h, WT and homozygous rats having either mutation 1 or 2 were anesthetized with isoflurane (Fujifilm Wako Pure Chemical Corp., Osaka, Japan), and their blood from the carotid artery and tissues were collected. The blood was allowed to clot overnight at 4 °C and then subjected to centrifugation at 2,700 × *g* for 10 min at 4 °C. Serum samples were stored at −80 °C until analysis. The excised tissues were frozen immediately in liquid nitrogen and stored at −80 °C until use.

The measurement of serum GH and IGF-I levels

The serum GH level was measured by a rat/mouse GH ELISA (ELISA) kit (catalog number EZRMGH-45K, EMD Millipore, Billerica, MA). The serum IGF-I level was measured

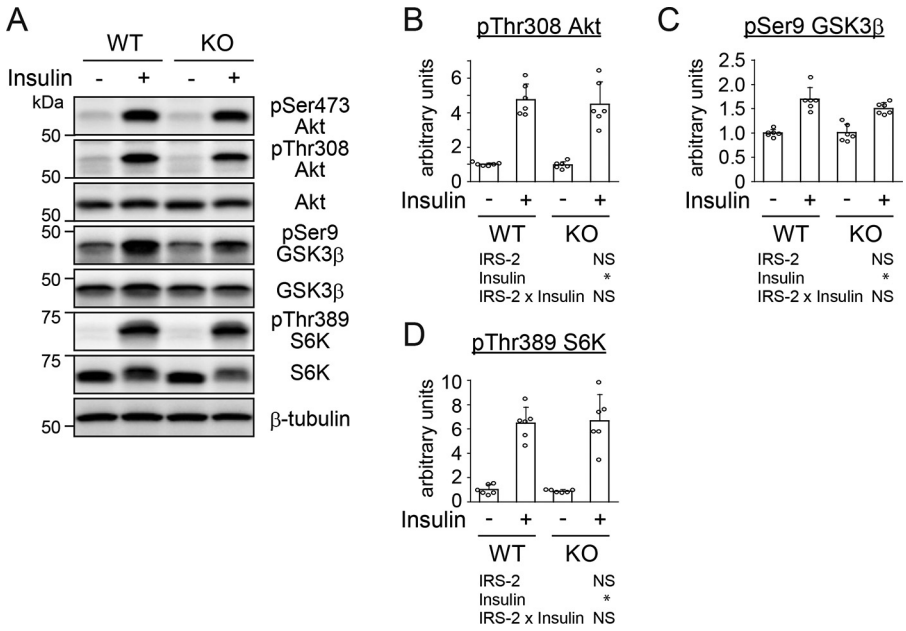

Figure 10. The insulin-simulated phosphorylation of Akt, GSK3β, and S6K in the skeletal muscle of male WT and IRS-2 KO rats. The 8-week–old male rats were treated as described in the legend to Fig. 7, and the skeletal muscle was dissected at 15 min after the insulin injection. *A–D*, insulin-stimulated phosphorylation of Akt, GSK3β, and S6K in the skeletal muscle. *A,* representative immunoblots. *B–D*, the immunoreactivity of Thr-308 phosphorylation of Akt (*B*), Ser-9 phosphorylation of GSK3β (*C*), and Thr-389 phosphorylation of S6K (*D*) was quantified and divided by the immunoreactivity of β-tubulin. Values are mean ± S.D. ($n = 6$). The two-way ANOVA results are below the graph (*, $p < 0.05$, *NS*, not significant).

by a mouse/rat IGF-I Quantikine ELISA kit (R&D Systems, Minneapolis, MN).

Glucose and insulin tolerance tests

A GTT was performed with 11- to 12-week–old rats. All rats were fasted for 4–5 h and then intraperitoneally injected with glucose solution (1.2 mg/kg BW). Approximately 30 μl of blood was obtained from tail vein using a heparinized microhematocrit capillary tube at 0, 15, 30, 60, and 120 min after glucose injection. The obtained blood sample was subjected to centrifugation at 2,700 × *g* for 10 min at 4 °C. Plasma samples were stored at −80 °C until analysis.

An ITT was performed with 12- to 13-week–old rats. All rats were fasted for 3–4 h and then intraperitoneally injected with bovine insulin (0.5 units/kg BW; Sigma-Aldrich). Blood was obtained from the tail vein at 0, 30, 60, 90, and 120 min after the insulin injection.

The blood glucose levels were measured with a glucometer (Ascensia Breeze, Bayer Medical, Leverkusen, Germany). Plasma insulin levels were measured by an ultra-sensitive mouse/rat insulin ELISA kit (Morinaga, Yokohama, Japan). We used the trapezoidal rule to calculate the incremental AUC for the changes in both blood glucose and plasma insulin levels during the GTT and the AAC for the changes in blood glucose levels during the ITT.

In vivo insulin stimulation

For the *in vivo* stimulation of insulin signaling, 8-week–old male rats were fasted overnight (14–16 h) and anesthetized with isoflurane (Fujifilm Wako). The abdominal cavity was then opened, and PBS or bovine insulin (0.5 units/kg of BW; Sigma-Aldrich) diluted in PBS was injected into the inferior vena cava. For our analysis of the early steps of insulin signaling, the liver was dissected at 1 min after insulin injection, and the skeletal muscle was dissected at 2 min after insulin injection.

To analyze the downstream of insulin signaling, we prepared a separate set of rats, and the liver and skeletal muscle were dissected at 15 min after insulin injection. The dissected tissues were immediately frozen in liquid nitrogen and stored at −80 °C until analysis.

RT-PCR analysis

The total RNA was prepared from the brain using TRIzol reagent (Thermo Fisher Scientific). To remove potential genomic DNA contamination, the RNA samples were treated with RNase-free DNase I and purified using RNeasy MinElute Cleanup kit (Qiagen, Valencia, CA). The cDNA was then synthesized from 2 μg of DNase-treated total RNA using SuperScript III (Thermo Fisher Scientific). The cDNA was diluted 1:10 with distilled water, and 1 μl from each sample was used for PCR. The primer sequences used were as follows: 5′-TCGATGTGAGAGGTGAGCAG-3′ and 5′-GCAATGAGGACAGGTGTGTG-3′ for amplifying fragment 1 of *Irs-2* (*Irs-2*_1; Fig. 1*B*), 5′-GAGACAACGACCAGTACGTGCT-3′ and 5′-TGTGGCAGCTGTTGCTGGAG-3′ for amplifying fragment 2 of *Irs-2* (*Irs-2_2*; Fig. 1*B*), and 5′-GGAGATTACTGCCCTGGCTCCTA-3′ and 5′-GACTCATCGTACTCCTGCTTGCTG-3′ for *Actb* as an internal control.

The preparation of protein extracts from tissues

The frozen tissues were homogenized with a Polytron homogenizer in ice-cold homogenizing buffer (50 mM HEPES-NaOH, pH 7.6, 10 mM sodium orthovanadate, 10 mM sodium pyrophosphate, 100 mM sodium fluoride, 2 mM phenylmethylsulfonyl

fluoride, 100 KIU/ml of aprotinin, 2 mM EDTA, and 2% Triton X-100). The homogenates were centrifuged at 100,000 × *g* for 1 h at 4 °C, and the supernatants were collected as protein extracts.

Immunoblotting

Equal amounts of protein sample were subjected to SDS-PAGE, and immunoblotting was performed as described (35). The bands of immunoreactive proteins were detected with an ECL kit (PerkinElmer Life Sciences, Boston, MA) and quantified using a cooled CCD camera system, the LAS-3000 mini (Fujifilm, Kanagawa, Japan). Anti-IRβ (C-19), anti-IRS-1 (C-20), and anti-IRS-2 (H-205) antibodies were purchased from Santa Cruz Biochemistry. Anti-phosphotyrosine 4G10 (No. 05-321), IRS-1 (No. 06-248), phospho-IRS-1 (Ser-307: No. 07-247), and IRS-2 (No. MABS15) antibodies were purchased from EMD Millipore (Temecula, CA). Anti-actin was purchased from Sigma. Anti-phospho-Akt (Thr-308: No. 4056, Ser-473: No. 4060), anti-Akt (No. 9272), anti-phospho-GSK3β (Ser-9: No. 9323), anti-GSK3β (No. 9315), anti-phospho-S6K (Thr-389: No. 9205), anti-S6K (No. 2708), and anti-β-tubulin (No. 2128) antibodies were purchased from Cell Signaling Technology (Danvers, MA).

To detect IRS-1 and IRS-2 protein in total protein extracts from the brain and epiWAT, 100 μg of protein sample was subjected to SDS-PAGE. After transblotting, the membranes were blocked with a blocking buffer (5% nonfat milk in TBS with Tween 20 (TBS-T: 10 mM Tris-HCl, pH 7.5, 100 mM NaCl, 0.1% Tween 20)) at room temperature for 1 h. The membranes were then incubated with anti-IRS-2 (H-205; Santa Cruz Biochemistry) antibody diluted in Can Get Signal® Solution 1 (TOYOBO, Osaka, Japan) at 4 °C overnight. After washing with TBS-T, the membranes were incubated with the appropriate horseradish peroxidase-conjugated secondary antibodies (GE Healthcare, Piscataway, NJ) diluted in Can Get Signal® Solution 2 (TOYOBO) at room temperature for 2 h, and washed again with TBS-T. The bands of immunoreactive IRS-1 and IRS-2 were detected as described above.

Immunoprecipitation

The protein extracts were immunoprecipitated with 1 μg of anti-IRβ (C-19), IRS-1 (C-20), or IRS-2 (H-205) antibodies (Santa Cruz Biochemistry) bound to protein G-Sepharose 4FF beads (GE Healthcare) as described (35, 36). According to the manufacturer's instructions, anti-IRS-2 antibody (H-205) could recognize the C-terminal region (amino acid sequence 926-1130 of human IRS-2 (total 1338 amino acids)) of IRS-2. Each immunoprecipitated sample was subjected to SDS-PAGE, followed by immunoblotting. We performed immunoblotting with both polyclonal anti-IRS-2 (H-205) and monoclonal anti-IRS-2 (MABS15) antibodies and confirmed that both polyclonal and monoclonal IRS-2 antibodies could detect IRS-2 protein similarly in the brain, liver, and skeletal muscle.

PI3K activity assay

The immunoprecipitated samples with anti-IRS-1 or IRS-2 antibody were washed with the homogenizing buffer, LiCl buffer (100 mM Tris-HCl, pH 7.5, 500 mM LiCl), distilled water, Tris-NaCl-EDTA buffer (10 mM Tris-HCl, pH 7.5, 150 mM NaCl, 1 mM EDTA), and reaction buffer (20 mM Tris-HCl, pH 7.5, 100 mM NaCl, 0.5 mM EGTA). The PI3K activity assay was conducted as described (37). The ^{32}P radioactivity incorporated into phosphatidylinositol was measured as the PI3K activity by Image J software (National Institutes of Health, Bethesda, MD).

Statistical analyses

All values are given as the mean ± S.D. When we compared two groups, the results were analyzed using unpaired Student's *t* test. The results for the changes of body weight, blood glucose level, and insulin level were analyzed by a two-way repeated measure analysis of variance (ANOVA). The results for insulin signaling were analyzed by a two-way factorial ANOVA. The Tukey-Kramer post-hoc test was performed when a significant interaction between factors was revealed by the two-way ANOVA. Differences were considered significant at $p < 0.05$.

Data availability

All data are contained within the article.

Acknowledgments—We thank Dr. Yusuke Taguchi, Dr. Takashi Yagi, and Kanako Oki for their help with animal care, and we appreciate the helpful discussions with Dr. Oksana Gavrilova (NIDDK, National Institutes of Health) during the preparation of this manuscript.

Author contributions— Y. T., K. N., H. K., K. Y. and S. M. validation; Y. T., K. N., R. T., N. T., and H. S. investigation; Y. T. and K. N. writing-original draft; Y. T., K. N., R. T., N. T., H. S., H. K., K. Y., and S. M. writing-review and editing.

Funding and additional information—This work was supported by Grant-in-Aid for Scientific Research Grants 16K07747 and 19K05916 (to Y. T.) from the Japan Society for the Promotion of Science.

Conflict of interest—The authors declare that they have no conflicts of interest.

Abbreviations—The abbreviations used are: IGF, insulin-like growth factor; IRS-2, insulin receptor substrate-2; PH, pleckstrin homology; mTOR, mammalian target of rapamycin; PTB, phosphotyrosine binding; PI3K, phosphatidylinositol 3-kinase; KO, knockout; epiWAT, epididymal white adipose tissues; BW, body weight; GH, growth hormone; GTT, glucose tolerance test; ITT, insulin tolerance test; AUC, area under the curve; AAC, area above the curve; IR, insulin receptor; sgRNA, single guide RNA; PIP, phosphatidylinositol; GSK3β, glycogen synthase kinase 3β; ANOVA, analysis of variance.

References

1. Saltiel, A. R., and Kahn, C. R. (2001) Insulin signalling and the regulation of glucose and lipid metabolism. *Nature* **414,** 799–806 CrossRef Medline

2. White, M. F. (2002) IRS proteins and the common path to diabetes. *Am. J. Physiol. Endocrinol. Metab.* **283,** E413–422 CrossRef Medline
3. Thirone, A. C., Huang, C., and Klip, A. (2006) Tissue-specific roles of IRS proteins in insulin signaling and glucose transport. *Trends Endocrinol. Metab.* **17,** 72–78 CrossRef Medline
4. Burks, D. J., Wang, J., Towery, H., Ishibashi, O., Lowe, D., Riedel, H., and White, M. F. (1998) IRS pleckstrin homology domains bind to acidic motifs in proteins. *J. Biol. Chem.* **273,** 31061–31067 CrossRef Medline
5. Yenush, L., Zanella, C., Uchida, T., Bernal, D., and White, M. F. (1998) The pleckstrin homology and phosphotyrosine binding domains of insulin receptor substrate 1 mediate inhibition of apoptosis by insulin. *Mol. Cell. Biol.* **18,** 6784–6794 CrossRef Medline
6. Withers, D. J., Gutierrez, J. S., Towery, H., Burks, D. J., Ren, J. M., Previs, S., Zhang, Y., Bernal, D., Pons, S., Shulman, G. I., Bonner-Weir, S., and White, M. F. (1998) Disruption of IRS-2 causes type 2 diabetes in mice. *Nature* **391,** 900–904 CrossRef Medline
7. Kubota, N., Tobe, K., Terauchi, Y., Eto, K., Yamauchi, T., Suzuki, R., Tsubamoto, Y., Komeda, K., Nakano, R., Miki, H., Satoh, S., Sekihara, H., Sciacchitano, S., Lesniak, M., Aizawa, S., *et al.* (2000) Disruption of insulin receptor substrate 2 causes type 2 diabetes because of liver insulin resistance and lack of compensatory beta-cell hyperplasia. *Diabetes* **49,** 1880–1889 CrossRef Medline
8. Kido, Y., Burks, D. J., Withers, D., Bruning, J. C., Kahn, C. R., White, M. F., and Accili, D. (2000) Tissue-specific insulin resistance in mice with mutations in the insulin receptor, IRS-1, and IRS-2. *J. Clin. Investig.* **105,** 199–205 CrossRef Medline
9. Araki, E., Lipes, M. A., Patti, M. E., Brüning, J. C., Haag, B., 3rd, Johnson, R. S., and Kahn, C. R. (1994) Alternative pathway of insulin signalling in mice with targeted disruption of the *IRS-1* gene. *Nature* **372,** 186–190 CrossRef Medline
10. Tamemoto, H., Kadowaki, T., Tobe, K., Yagi, T., Sakura, H., Hayakawa, T., Terauchi, Y., Ueki, K., Kaburagi, Y., and Satoh, S. and (1994) Insulin resistance and growth retardation in mice lacking insulin receptor substrate-1. *Nature* **372,** 182–186 CrossRef Medline
11. Yamauchi, T., Tobe, K., Tamemoto, H., Ueki, K., Kaburagi, Y., Yamamoto-Honda, R., Takahashi, Y., Yoshizawa, F., Aizawa, S., Akanuma, Y., Sonenberg, N., Yazaki, Y., and Kadowaki, T. (1996) Insulin signalling and insulin actions in the muscles and livers of insulin-resistant, insulin receptor substrate 1-deficient mice. *Mol. Cell. Biol.* **16,** 3074–3084 CrossRef Medline
12. Cong, L., Ran, F. A., Cox, D., Lin, S., Barretto, R., Habib, N., Hsu, P. D., Wu, X., Jiang, W., Marraffini, L. A., and Zhang, F. (2013) Multiplex genome engineering using CRISPR/Cas systems. *Science* **339,** 819–823 CrossRef Medline
13. Mali, P., Yang, L., Esvelt, K. M., Aach, J., Guell, M., DiCarlo, J. E., Norville, J. E., and Church, G. M. (2013) RNA-guided human genome engineering via Cas9. *Science* **339,** 823–826 CrossRef Medline
14. Li, D., Qiu, Z., Shao, Y., Chen, Y., Guan, Y., Liu, M., Li, Y., Gao, N., Wang, L., Lu, X., Zhao, Y., and Liu, M. (2013) Heritable gene targeting in the mouse and rat using a CRISPR-Cas system. *Nat. Biotechnol.* **31,** 681–683 CrossRef Medline
15. Li, W., Teng, F., Li, T., and Zhou, Q. (2013) Simultaneous generation and germline transmission of multiple gene mutations in rat using CRISPR-Cas systems. *Nat. Biotechnol.* **31,** 684–686 CrossRef Medline
16. Copps, K. D., and White, M. F. (2012) Regulation of insulin sensitivity by serine/threonine phosphorylation of insulin receptor substrate proteins IRS1 and IRS2. *Diabetologia* **55,** 2565–2582 CrossRef Medline
17. Um, S. H., Frigerio, F., Watanabe, M., Picard, F., Joaquin, M., Sticker, M., Fumagalli, S., Allegrini, P. R., Kozma, S. C., Auwerx, J., and Thomas, G. (2004) Absence of S6K1 protects against age- and diet-induced obesity while enhancing insulin sensitivity. *Nature* **431,** 200–205 CrossRef Medline
18. Carlson, C. J., White, M. F., and Rondinone, C. M. (2004) Mammalian target of rapamycin regulates IRS-1 serine 307 phosphorylation. *Biochem. Biophys. Res. Commun.* **316,** 533–539 CrossRef Medline
19. Rui, L., Aguirre, V., Kim, J. K., Shulman, G. I., Lee, A., Corbould, A., Dunaif, A., and White, M. F. (2001) Insulin/IGF-1 and TNF-α stimulate phosphorylation of IRS-1 at inhibitory Ser307 via distinct pathways. *J. Clin. Investig.* **107,** 181–189 CrossRef Medline
20. Shah, O. J., and Hunter, T. (2006) Turnover of the active fraction of IRS1 involves raptor-mTOR- and S6K1-dependent serine phosphorylation in cell culture models of tuberous sclerosis. *Molecular and cellular biology* **26,** 6425–6434 CrossRef Medline
21. Le Roith, D., Bondy, C., Yakar, S., Liu, J. L., and Butler, A. (2001) The somatomedin hypothesis: 2001. *Endocr. Rev.* **22,** 53–74 CrossRef Medline
22. Lin, X., Taguchi, A., Park, S., Kushner, J. A., Li, F., Li, Y., and White, M. F. (2004) Dysregulation of insulin receptor substrate 2 in beta cells and brain causes obesity and diabetes. *J. Clin. Investig.* **114,** 908–916 CrossRef Medline
23. Kubota, N., Terauchi, Y., Tobe, K., Yano, W., Suzuki, R., Ueki, K., Takamoto, I., Satoh, H., Maki, T., Kubota, T., Moroi, M., Okada-Iwabu, M., Ezaki, O., Nagai, R., Ueta, Y., *et al.* (2004) Insulin receptor substrate 2 plays a crucial role in beta cells and the hypothalamus. *J. Clin. Investig.* **114,** 917–927 CrossRef Medline
24. Withers, D. J., Burks, D. J., Towery, H. H., Altamuro, S. L., Flint, C. L., and White, M. F. (1999) Irs-2 coordinates Igf-1 receptor-mediated beta-cell development and peripheral insulin signalling. *Nat. Genet.* **23,** 32–40 CrossRef Medline
25. Boura-Halfon, S., and Zick, Y. (2009) Phosphorylation of IRS proteins, insulin action, and insulin resistance. *Am. J. Physiol. Endocrinol. Metab.* **296,** E581–E591 CrossRef Medline
26. Burks, D. J., Font de Mora, J., Schubert, M., Withers, D. J., Myers, M. G., Towery, H. H., Altamuro, S. L., Flint, C. L., and White, M. F. (2000) IRS-2 pathways integrate female reproduction and energy homeostasis. *Nature* **407,** 377–382 CrossRef Medline
27. Schubert, M., Brazil, D. P., Burks, D. J., Kushner, J. A., Ye, J., Flint, C. L., Farhang-Fallah, J., Dikkes, P., Warot, X. M., Rio, C., Corfas, G., and White, M. F. (2003) Insulin receptor substrate-2 deficiency impairs brain growth and promotes tau phosphorylation. *J. Neurosci.* **23,** 7084–7092 CrossRef
28. White, M. F. (2014) IRS2 integrates insulin/IGF1 signalling with metabolism, neurodegeneration and longevity. *Diabetes Obesity Metab.* **16, Suppl. 1,** 4–15 CrossRef Medline
29. Irvine, E. E., Drinkwater, L., Radwanska, K., Al-Qassab, H., Smith, M. A., O'Brien, M., Kielar, C., Choudhury, A. I., Krauss, S., Cooper, J. D., Withers, D. J., and Giese, K. P. (2011) Insulin receptor substrate 2 is a negative regulator of memory formation. *Learn. Memory* **18,** 375–383 CrossRef Medline
30. Sadagurski, M., Cheng, Z., Rozzo, A., Palazzolo, I., Kelley, G. R., Dong, X., Krainc, D., and White, M. F. (2011) IRS2 increases mitochondrial dysfunction and oxidative stress in a mouse model of Huntington disease. *J. Clin. Investig.* **121,** 4070–4081 CrossRef Medline
31. Costello, D. A., Claret, M., Al-Qassab, H., Plattner, F., Irvine, E. E., Choudhury, A. I., Giese, K. P., Withers, D. J., and Pedarzani, P. (2012) Brain deletion of insulin receptor substrate 2 disrupts hippocampal synaptic plasticity and metaplasticity. *PLoS One* **7,** e31124 CrossRef Medline
32. Martín, E. D., Sanchez-Perez, A., Trejo, J. L., Martin-Aldana, J. A., Cano Jaimez, M., Pons, S., Acosta Umanzor, C., Menes, L., White, M. F., and Burks, D. J. (2012) IRS-2 deficiency impairs NMDA receptor-dependent long-term potentiation. *Cereb. Cortex* **22,** 1717–1727 CrossRef Medline
33. Fujii, W., Kawasaki, K., Sugiura, K., and Naito, K. (2013) Efficient generation of large-scale genome-modified mice using gRNA and CAS9 endonuclease. *Nucleic Acids Res.* **41,** e187 CrossRef Medline
34. Nakamura, K., Fujii, W., Tsuboi, M., Tanihata, J., Teramoto, N., Takeuchi, S., Naito, K., Yamanouchi, K., and Nishihara, M. (2014) Generation of muscular dystrophy model rats with a CRISPR/Cas system. *Sci. Rep.* **4,** 5635 CrossRef Medline
35. Toyoshima, Y., Tokita, R., Ohne, Y., Hakuno, F., Noguchi, T., Minami, S., Kato, H., and Takahashi, S. (2010) Dietary protein deprivation upregulates

insulin signaling and inhibits gluconeogenesis in rat liver. *J. Mol. Endocrinol.* **45,** 329–340 CrossRef Medline

36. Toyoshima, Y., Ohne, Y., Takahashi, S. I., Noguchi, T., and Kato, H. (2004) Dietary protein deprivation decreases the serine phosphorylation of insulin receptor substrate-1 in rat skeletal muscle. *J. Mol. Endocrinol.* **32,** 519–531 CrossRef Medline

37. Shibata, M., Hakuno, F., Yamanaka, D., Okajima, H., Fukushima, T., Hasegawa, T., Ogata, T., Toyoshima, Y., Chida, K., Kimura, K., Sakoda, H., Takenaka, A., Asano, T., and Takahashi, S. (2010) Paraquat-induced oxidative stress represses phosphatidylinositol 3-kinase activities leading to impaired glucose uptake in 3T3-L1 adipocytes. *J. Biol. Chem.* **285,** 20915–20925 CrossRef Medline